

1           Large deformation numerical modeling of the short-term  
2           compression and uplift capacity of offshore shallow foundations

3

4   Santiram CHATTERJEE, M.Tech, PhD  
5   Centre for Offshore Foundation Systems, (M053) and ARC Centre of Excellence for  
6   Geotechnical Science and Engineering,  
7   The University of Western Australia  
8   35 Stirling Highway, Crawley, WA – 6009, Australia  
9   Email: [santiram.chatterjee@uwa.edu.au](mailto:santiram.chatterjee@uwa.edu.au)

10

11   Divya S. K. MANA, B.Tech, M.Tech  
12   Centre for Offshore Foundation Systems (M053) and ARC Centre of Excellence for  
13   Geotechnical Science and Engineering,  
14   The University of Western Australia  
15   35 Stirling Highway, Crawley, WA – 6009, Australia  
16   Email: [20674905@student.uwa.edu.au](mailto:20674905@student.uwa.edu.au)

17

18   Susan GOURVENEK, B.Eng, PhD (corresponding author)  
19   Centre for Offshore Foundation Systems, (M053) and ARC Centre of Excellence for  
20   Geotechnical Science and Engineering, The University of Western Australia  
21   35 Stirling Highway, Crawley, WA – 6009, Australia  
22   Tel: +61 8 6488 3995  
23   Fax: +61 8 6488 1044  
24   Email: [susan.gourvenec@uwa.edu.au](mailto:susan.gourvenec@uwa.edu.au)

25

26   Mark F. RANDOLPH, M.A., PhD  
27   Centre for Offshore Foundation Systems, (M053) and ARC Centre of Excellence for  
28   Geotechnical Science and Engineering, The University of Western Australia  
29   35 Stirling Highway, Crawley, WA – 6009, Australia  
30   Email: [mark.randolph@uwa.edu.au](mailto:mark.randolph@uwa.edu.au)

31

32   No. of words: 4309 (introduction to conclusions inclusive)

33   No. of tables: 2

34   No. of figures: 8

35

## 36 ABSTRACT

37 Large deformation finite element analysis has been used to model the undrained  
38 response of skirted shallow foundations in uplift and compression. Large deformation  
39 effects involve changes in embedment ratio and operative local soil shear strength  
40 with increasing foundation displacement – either in tension or compression.  
41 Centrifuge model testing has shown that these changes in geometry affect the  
42 mobilised bearing capacity and the kinematic mechanisms governing failure in  
43 undrained uplift and compression. Small strain finite element analysis cannot by  
44 definition capture the effects of changing foundation embedment ratio and variation in  
45 local soil strength with foundation displacement. In this paper, load-displacement  
46 relationships, ultimate capacities and kinematic mechanisms governing failure from  
47 large deformation finite element analyses are compared with centrifuge model test  
48 results for circular skirted foundations with a range of embedment between 10 % and  
49 50 % of the foundation diameter.

50 The results show that the large deformation finite element method can replicate the  
51 load-displacement response of the foundations over large displacements, pre- and  
52 post-yield, and also capture differences in the soil deformation patterns in uplift and  
53 compression. The findings from this study increase confidence in using advanced  
54 numerical methods for determining shallow skirted foundation behavior, particularly  
55 for load paths involving uplift.

56

## 57 INTRODUCTION

58 Shallow skirted foundations comprise a foundation plate that rests on the seabed with  
59 a peripheral skirt and sometimes internal skirts that penetrate into the seabed,

60 confining a soil plug. Shallow skirted foundations are an attractive solution for many  
61 offshore applications, including fixed bottom or buoyant platforms, subsea  
62 infrastructure for wells and pipelines, and increasingly for renewable energy  
63 applications (e.g. Bye et al., 1995; Watson & Humpheson, 2007; Christophersen et  
64 al., 1992; Miller et al., 1996; Dendani & Colliat, 2002; Gaudin et al., 2011). A key  
65 advantage of skirted foundations is their ability to resist short-term tensile loads due  
66 to generation of negative excess pore pressure, also referred to as suction (relative to  
67 ambient water pressure), inside the skirt compartment during undrained pullout.  
68 Suction enables mobilization of reverse end bearing capacity i.e. a general shear  
69 failure mode as observed under compression, but in reverse. When reverse end  
70 bearing is mobilized, uplift capacity equivalent to the compression capacity is  
71 expected (Watson et al. 2000; Mana et al. 2012b). In the absence of suction, uplift  
72 resistance is derived only from the frictional resistance mobilized along the skirt-soil  
73 interface, which may be up to an order of magnitude less than reverse end bearing  
74 capacity.

75 Several experimental studies have reported reverse end bearing of skirted foundations  
76 (Puech et al., 1993; Watson et al., 2000; Gourvenec et al., 2009, Mana et al., 2011,  
77 2012a, b). Experimental studies must achieve stress similitude between model and  
78 prototype conditions in order for reverse end bearing to be realized (Puech et al.,  
79 1993). As a result, model tests must be carried out in a geotechnical centrifuge which  
80 imposes constraints over the number of tests, the applied loading paths and loading  
81 sequences owing to space restrictions and hardware capability.

82 Numerical analysis is an attractive method of augmenting physical model  
83 programmes to consider load paths or other conditions that would be impossible or

84 impractical to model in the centrifuge. In Total Lagrangian, i.e. small strain finite  
85 element (SSFE) analysis the nodes of the mesh move with the associated material  
86 point and all the variables are referred to the undeformed geometry. Hence SSFE  
87 analysis cannot for example, capture higher strength of deeper soil or lower strength  
88 of the shallower soil as a foundation is penetrated downwards or pulled out. In other  
89 words, SSFE analysis cannot by definition capture effects associated with changing  
90 geometry and therefore cannot distinguish between a skirted foundation in undrained  
91 compression and uplift when reverse end bearing is mobilized. Total Lagrangian  
92 analyses are also limited by gross mesh distortion or entanglement due to large  
93 movements, particularly in the finely meshed region around the skirt tip.  
94 Shortcomings of SSFE analysis to capture the kinematic failure mechanisms of  
95 shallow skirted foundations in undrained uplift and compression were explicitly  
96 illustrated by Mana et al. (2012) through comparison with centrifuge test data. The  
97 SSFE analyses were shown to represent the failure mechanisms in undrained  
98 compression reasonably but since, by definition of small strain analyses, the response  
99 in fully-bonded undrained uplift was identical but reversed in sense to that in  
100 compression, the uplift mechanisms observed in the centrifuge model tests were  
101 poorly represented.

102 In order to explore the full load-displacement response and any differences in failure  
103 mechanisms between undrained uplift and compression, it is important to capture the  
104 geometric and material non-linearity associated with large deformations. Numerical  
105 modeling of large deformation problems can be achieved using a finite element  
106 methodology based on the “remeshing and interpolation technique with small strain”  
107 (RITSS) approach developed by Hu & Randolph (1998a, b). This analysis technique  
108 has previously been adopted successfully to study the large displacement behavior of

109 offshore foundations, penetrometers and pipelines (Hu et al., 1999; Zhou & Randolph,  
110 2006, 2007; Hossain & Randolph, 2010; Wang et al., 2010a, 2010b; Chatterjee et al.,  
111 2012). To the authors' knowledge, the undrained compression and uplift response of  
112 skirted foundations have not previously been considered by large deformation finite  
113 element (LDFE) analysis.

114 LDFE analysis offers the potential to augment physical modeling programmes if it  
115 can be shown that the numerical method can adequately predict the observed  
116 responses. The study presented in this paper uses LDFE analysis to back analyze  
117 centrifuge test results for circular shallow skirted foundations with a range of  
118 foundation embedment between 10 % and 50 % of the foundation diameter. The  
119 results of the LDFE analysis are compared with data from two programmes of  
120 centrifuge tests. One programme of centrifuge tests modeled a complete circular  
121 skirted foundation under undrained compression and uplift, which yielded the  
122 complete load-displacement response over large displacements (Mana et al. 2012). A  
123 second programme of centrifuge tests modeled a 'half' circular foundation that was  
124 tested against a Perspex window (Mana et al. 2013). Digital imaging and particle  
125 image velocimetry (PIV, White et al. 2003) was used to define the soil flow vectors  
126 during undrained compression and uplift enabling the kinematic mechanisms  
127 associated with failure to be identified.

## 128 LARGE DEFORMATION FINITE ELEMENT MODELING

### 129 *Methodology*

130 Remeshing and interpolation technique with small strain (RITSS, Hu & Randolph,  
131 1998a, 1998b) falls under the category of Arbitrary Lagrangian Eulerian formulation  
132 (ALE, Ghosh & Kikuchi, 1991), in which mesh and material displacements are

133 uncoupled to avoid severe mesh distortion in large deformation problems. In this  
134 methodology, a series of small strain Lagrangian analyses are conducted with the soil  
135 being remeshed and the stresses and material properties mapped after each small  
136 strain analysis. Recently, Wang et al. (2010a, 2010b) implemented RITSS in the  
137 commercial software Abaqus (Dassault Systèmes, 2010) due to its powerful mesh  
138 generation tools and computational efficiency. The same numerical methodology is  
139 adopted for the present study, but with some problem specific developments and  
140 modifications. The analysis procedure is carried out using a master Fortran program.  
141 Python scripts, the in-built scripting language of Abaqus, are used for pre-processing  
142 and post-processing different analyses. The master program calls various subroutines  
143 and Python scripts repeatedly, displacing the foundation incrementally, remeshing and  
144 mapping field variables between increments, until the required large displacement is  
145 achieved.

#### 146 *Finite element model*

147 Fig. 1 shows a typical axisymmetric finite element model created for the LDFE  
148 analyses. The foundations were modeled with prototype dimensions  $D = 12$  m,  $d/D =$   
149  $0.1, 0.2, 0.3$  and  $0.5$ ,  $t/D = 0.008$ , replicating the foundations that were tested in the  
150 centrifuge (Mana et al. 2013). The radial extent and depth of the soil domain was  
151 defined at a distance of eight times the radius of the foundation from the centre of the  
152 underside of the foundation top plate. The vertical soil boundary was restrained  
153 against radial movement and the bottom boundary was restrained against movement  
154 in radial and vertical directions. 6-node quadratic triangular axisymmetric elements  
155 from the Abaqus standard library (CAX6) were chosen for discretization of the soil.  
156 The foundation was defined as a rigid body.

157 The skirt-soil interface was assumed to have fully rough contact with no separation  
158 allowed in the normal direction. In practice, some reduction in shear strength may  
159 exist at the skirt-soil interface, particularly for a metallic skirt as modeled in the  
160 centrifuge tests. However, representation of partial interface roughness is impractical  
161 in the LDFE analyses. Interface elements in Abaqus cannot be prescribed constant  
162  $\alpha s_u$ -type strength reduction (with  $0 < \alpha < 1$ ), so a thin layer of elements must be  
163 incorporated along the foundation-soil interface and explicitly prescribed a reduced  
164 shear strength. This method has been adopted successfully in small strain finite  
165 element analyses (e.g. Supachawarote et al., 2004; Gourvenec & Barnett, 2011;  
166 Gourvenec & Mana, 2011), but a very thin layer of a material with different properties  
167 to the rest of the continuum is impractical for large deformation analysis.

168 An unlimited tension interface along the underside of the foundation base plate was  
169 selected to represent the suction capacity available when a skirted foundation is fully  
170 sealed. An unlimited tension interface was also prescribed along the internal and  
171 external vertical skirt-soil interface, since, as only vertical loading was considered,  
172 tensile forces would not be transmitted to the vertical sides of the skirts and the  
173 prescribed tensile interface would not be activated. The modeled foundation  
174 parameters are summarized in Table 1.

#### 175 *Soil parameters*

176 The LDFE analyses are based on a basic linear elastic perfectly plastic Tresca  
177 constitutive model with inclusion of strain rate and strain softening effects by  
178 modifying the value of undrained shear strength after each small strain step.

179 Einav & Randolph (2005) proposed an expression for the modified shear strength ( $s_u$ )  
180 of soil incorporating the combined effects of strain rate and strain softening given by

181 
$$s_u = \left[ 1 + \mu \log \left( \frac{\max(\dot{\gamma}_{\max}, \dot{\gamma}_{\text{ref}})}{\dot{\gamma}_{\text{ref}}} \right) \right] \left[ \delta_{\text{rem}} + (1 - \delta_{\text{rem}}) e^{-3\varepsilon/\varepsilon_{95}} \right] s_{\text{ui}} \quad (1)$$

182 where  $s_{\text{ui}}$  is the original intact shear strength at and below the reference strain rate  
 183  $\dot{\gamma}_{\text{ref}}$ . The first part of the equation takes account of the effect of strain rate and the  
 184 second part takes account of strain softening of the soil. In Eq. (1),  $\mu$  is the rate  
 185 parameter or the rate of increase in strength per decade, typically taken as a value  
 186 between 0.05 and 0.2 (Biscontin & Pestana, 2001; Lunne & Andersen, 2007). The  
 187 maximum shear strain rate is defined as

188 
$$\dot{\gamma}_{\max} = \frac{(\Delta\varepsilon_1 - \Delta\varepsilon_3) v_f}{\delta/D} \frac{v_f}{D} \quad (2)$$

189 where  $\delta$  is the incremental displacement of the foundation,  $\Delta\varepsilon_1$  and  $\Delta\varepsilon_3$  are  
 190 respectively the resulting major and minor principal strains,  $v_f$  is the foundation  
 191 displacement rate and  $D$  is the diameter of the foundation. The value of reference  
 192 shear strain rate may be related to laboratory values, typically from 1 to 4 % per hour  
 193 for triaxial tests and 5 to 20 % per hour for simple shear tests (Erbrich, 2005; Lunne et  
 194 al., 2006; Lunne & Andersen, 2007). Here the minimum value of reference strain,  
 195  $\dot{\gamma}_{\text{ref}} = 1$  % per hour, was chosen, as has been adopted in previous numerical and  
 196 analytical studies (Einav & Randolph, 2005; Zhou & Randolph, 2007; Wang et al.,  
 197 2010a; Chatterjee et al., 2012). For calculation of the maximum shear strain rate, the  
 198 foundation diameter  $D$  and foundation velocity  $v_f$ , were taken from the centrifuge  
 199 model test conditions, a very small value of incremental foundation displacement  $\delta =$   
 200  $0.0008D$  was selected, and  $\Delta\varepsilon_1$  and  $\Delta\varepsilon_3$  were extracted from the output file after each  
 201 step of the analysis.



202 The second part of Eq. (1) accounts for the effect of softening of the soil.  $\delta_{rem}$  is the  
203 reciprocal of sensitivity ( $S_t$ ) of soil, i.e., the ratio of fully remolded to intact shear  
204 strength of soil. In this study,  $\delta_{rem}$  was calculated from cyclic T-bar tests carried out in  
205 the centrifuge soil sample (as described in Andersen et al., 2005).  $\xi$  is the accumulated  
206 absolute plastic strain at the integration points, while  $\xi_{95}$  is the cumulative shear strain  
207 for 95 % shear strength degradation, with typical values ranging from 10 to 50  
208 (Randolph, 2004).

209 Rate parameter  $\mu$  and remolding parameter  $\xi_{95}$  were not ascertained for the centrifuge  
210 tests with which the LDFE analysis results are compared. These values were selected  
211 through a parametric study (described in the following section) to give good  
212 agreement with a selected centrifuge test result. The same soil parameters were  
213 applied in all the back analyses, i.e. the values of the parameters were not individually  
214 fitted for each foundation embedment ratio and load path. The selected values fall  
215 within the ranges identified in previous published studies (Biscontin & Pestana, 2001;  
216 Randolph, 2004; Einav & Randolph, 2005; Lunne & Andersen, 2007).

217 The best-fit linear shear strength profile measured in the centrifuge tests with the  
218 miniature T-bar penetrometer (Mana et al., 2012b) was used as the base-line strength  
219 in the LDFE analyses, as defined in Table 1. Equation 1 was used to define the  
220 modified shear strength of soil after each small strain analysis step.

221 A value close to the undrained Poisson's ratio,  $\nu_u = 0.49$ , rather than 0.5, was adopted  
222 to avoid numerical problems associated with modeling incompressible materials. The  
223 foundation and soil parameters used in the LDFE analyses are summarized in Table 1.

## 224 RESULTS

225 The results of the parametric LDFE analyses used to identify the input parameters  
226 used in the main programme of LDFE analyses are presented first followed by a  
227 comparison of LDFE results with centrifuge model test results defining the load-  
228 displacement response, ultimate (reverse) bearing capacity and kinematic failure  
229 mechanisms.

### 230 *Parametric LDFE analyses*

231 Parametric analyses were carried out to assess the effect of stiffness ratio,  $E_u/s_u$ , rate  
232 parameter,  $\mu$ , and remolding parameter,  $\xi_{95}$ , on the load-displacement response of the  
233 foundations to identify the best-fit values to represent the centrifuge test results. A  
234 single set of parameters for the LDFE analyses was selected based on best-fit with the  
235 observed load-displacement response and ultimate bearing capacity for a selected case  
236 of the foundation with embedment ratio  $d/D = 0.1$  in undrained compression. The  
237 same parameters were used to back-analyze the response of foundations with a range  
238 of embedment ratios in both compression and uplift.

239 Fig. 2 a-c shows the effect of the value of  $E_u/s_u$ ,  $\mu$  and  $\xi_{95}$  respectively on the  
240 calculated load-displacement response and ultimate bearing capacity for the selected  
241 case of the skirted foundation with embedment ratio  $d/D = 0.1$ , with all other  
242 parameters as given in Table 1. The vertical co-ordinate is the displacement ( $w$ ) of the  
243 foundation from the installation position, normalized by the foundation diameter ( $D$ ).  
244 The horizontal co-ordinate defines the normalized bearing response,  $q_{net}/s_{u0}$ , with  $q_{net}$   
245 calculated as

$$246 \quad q_{net} = \frac{F}{A} - \gamma'(d + w) + \frac{W_{soilplug}}{A} \quad (3)$$

247 Here,  $F$  is the reaction force measured at the reference point of the foundation during  
 248 compression or uplift,  $A$  is the outer cross sectional area of the skirt,  $\gamma'$  is the effective  
 249 unit weight of soil,  $d$  is the skirt embedment depth and  $W_{\text{soilplug}}$  is the weight of the  
 250 soil plug inside the skirt compartment ( $W_{\text{soilplug}}/A = \gamma'd$ ). The capacity of the  
 251 foundation in uplift or compression is defined in terms of a bearing capacity factor,  
 252  $N_{c0}$ , as

$$253 \quad N_{c0} = \frac{q_{\text{net}}}{s_{u0,\text{tip}}} \quad (4)$$

254 where  $s_{u0,\text{tip}}$  is the initial shear strength at the skirt tip level.

255 A clear dependence of foundation response on all the parameters can be observed  
 256 from Fig. 2. The bearing capacity response at low displacements is mostly affected by  
 257 soil stiffness both in compression and uplift and at larger displacements by strain rate  
 258 and strain softening. Increased strain rate leads to increased bearing capacity and  
 259 increased remolding parameter leads to more rapid softening or hardening. Stiffness  
 260 ratio  $E_u/s_u = 400$ , rate of shear strength increase per decade  $\mu = 0.1$  and cumulative  
 261 shear strain for 95 % shear strength degradation  $\xi_{95} = 10$  were selected for the full  
 262 suite of LDFE analyses (see Table 1) based on good agreement with the load-  
 263 displacement response in compression observed in the centrifuge for the foundation  
 264 with  $d/D = 0.1$ , also included in Fig. 2.

265 It should be noted that, since the exact values of parameters  $\mu$  and  $\xi_{95}$  were not  
 266 measured for the experimental study, the values obtained through parametric study  
 267 may not be a unique set. For example, the parameters will vary with the value of the  
 268 foundation-soil interface roughness in order to match the observed resistance.  
 269 Nonetheless, the selected values fall within expected ranges (Biscontin & Pestana,

270 2001; Randolph, 2004; Einav & Randolph, 2005; Lunne & Andersen, 2007) and the  
271 same set of parameters was used in all the back analyses.

### 272 *Bearing response*

273 Fig. 3 a-d compares the normalized bearing response predicted from the LDFE  
274 analyses (calculated with the input parameters given in Table 1) with observations  
275 from centrifuge tests, reported by Mana et al. (2012b). Lower and upper bound  
276 solutions for rough-sided, rough-based circular foundations and  $kD/s_{um} = 2$  (similar to  
277 the degree of soil heterogeneity in this study) are also shown (Martin, 2001).

278 Fig. 3 indicates a similar load-displacement response in compression for all the  
279 foundation embedment ratios observed in the centrifuge tests and predicted by the  
280 LDFE analyses. Resistance gradually develops until the bearing capacity is mobilized  
281 after which resistance continues to increase only in line with the increase in shear  
282 strength with further penetration. The strain rate effect dominates initially, increasing  
283 the soil bearing capacity. At larger displacements, the strain rate effect is balanced,  
284 and eventually overpowered, by the effect of soil softening due to accumulation of  
285 plastic strain. The predicted initial bearing capacities fall within the bounds of the  
286 theoretical predictions. The theoretical predictions are based on assumptions of small  
287 strain and are therefore independent of foundation displacement. In other words, only  
288 a single value of bearing capacity is predicted, corresponding to the initial embedment  
289 ratio and corresponding tip level shear strength.

290 The response in compression from the LDFE analyses for  $d/D = 0.1$  coincides with  
291 the centrifuge test data as would be expected since this test was chosen as the  
292 selection criterion for the stiffness, rate and ductility parameters. Good agreement  
293 with the centrifuge test data is observed in the initial stiffness response in  
294 compression in the LDFE analyses with other embedment ratios. The load-

295 displacement response is under-predicted by the LDFE analysis with increasing  
296 foundation displacement. The higher bearing resistance observed in the centrifuge  
297 tests in compression compared to that predicted by the LDFE analyses may have  
298 resulted from an increase in the operative shear strength of the soil arising from  
299 consolidation during the waiting period following installation in the centrifuge tests  
300 that was not represented in the LDFE analyses.

301 In uplift, resistance is gradually mobilized with increasing displacement until a peak,  
302 which is followed by (a generally) stable, but diminishing capacity as (i) embedment  
303 is lost and (ii) the foundation moves into the softer shallower soil. Beyond some  
304 critical displacement suction beneath the top plate is spontaneously lost, which  
305 corresponds to rapid loss of uplift resistance. The LDFE results over-predict the peak  
306 bearing capacity at low embedment ratio and under predict at the higher embedment  
307 ratio,  $d/D = 0.5$  with a consistent trend of reducing over-prediction and then  
308 increasing under-prediction with increasing embedment ratio.

309 The LDFE analyses under-predict the rate of decrease in bearing capacity with  
310 foundation displacement following peak capacity. This is likely to be due to the fully  
311 bonded interface condition between the external skirt and soil. In reality the soil  
312 adjacent to the foundation will be pulled down as the foundation displaces upwards  
313 (by virtue of the constant volume condition) such that the loss of embedment is more  
314 severe than that due only to foundation displacement. The effect is more significant at  
315 lower embedment ratios. The proportional reduction in embedment due to downward  
316 movement is less severe with increasing initial embedment ratio.

317 The LDFE analyses were not able to replicate the loss of suction at the foundation-soil  
318 interface, resulting in the sudden loss of uplift resistance seen in Fig. 3a and b. The

319 fully bonded interface between top plate and soil prescribed in the LDFE analyses  
320 ensured that unlimited suction could be maintained at any displacement.

321 Loss of suction was observed particularly early in the centrifuge test of the foundation  
322 with the lowest embedment ratio,  $d/D = 0.1$ . It is considered that this was due to loss  
323 of sealing in the experiment and so is not expected to be captured by the LDFE  
324 analysis.

325 Fig. 4 demonstrates the effect of varying stiffness, ductility and rate parameters (all  
326 other parameters being kept constant) for the foundation with embedment ratio  $d/D =$   
327  $0.5$ . It is clear that a better fit can be achieved by adjusting the soil parameters. This  
328 is not necessarily unexpected since slight variations in shear strength at the different  
329 locations or time of each centrifuge test may have influenced the load-displacement  
330 response.

### 331 ***Bearing capacity factors***

332 Bearing capacity factors (adopting the same terminology for uplift) predicted by the  
333 LDFE analyses and observed in the centrifuge tests are summarized in Table 2,  
334 together with the measured normalised displacements,  $w/D$ , at which the peak  
335 resistance was mobilized. In uplift, the point of failure is unambiguous. However,  
336 there is some ambiguity as to the value selected to represent compression capacity; if  
337 it is (i) the steady state value (where increase in resistance is due only to the increase  
338 in shear strength), (ii) the value at a specified foundation displacement (e.g. 5 or 10 %  
339 of the foundation diameter), or (iii) the value at the equivalent magnitude of  
340 displacement that the peak uplift resistance was mobilized. In Table 2, the bearing  
341 capacity factor in compression is taken at a fixed displacement of  $w/D = 0.05$ , by  
342 which stage the resistance has either reached a plateau or a steady increase according  
343 to the increasing shear strength with depth. Lower bound (LB) and upper bound (UB)

344 solutions for rough-sided, rough-based circular foundations for  $kD/s_{um} = 2$  (Martin,  
345 2001) are also stated in Table 2. Similar magnitudes of bearing capacity factors were  
346 predicted by the LDFE analyses compared with the centrifuge results in both  
347 compression and uplift, with an absolute average difference of 5 %.

348 Bearing capacity factors predicted from SSFE analyses are also shown in Table 2. The  
349 values are identical in compression and uplift due to the small strain conditions and  
350 fully bonded foundation-soil interface. The peak bearing capacity factors predicted  
351 from the SSFE analyses are similar to those in the centrifuge tests, the LDFE analyses  
352 and the bound solutions. However, the SSFE analyses predict a constant bearing  
353 capacity with increased foundation displacement (either upwards or downwards) and  
354 cannot model the changing bearing capacity with changing foundation embedment as  
355 captured by the LDFE analyses.

### 356 *Failure Mechanisms*

357 Fig. 5a and b compare soil displacement vectors for foundations with embedment  
358 ratios  $d/D = 0.1$  and  $0.5$  predicted by the LDFE analyses and observed in the half-  
359 model centrifuge tests presented by Mana et al. (2012a). In uplift, even for the  
360 shallow embedment ratio of  $d/D = 0.1$ , soil around the entire foundation is mobilized  
361 rather than just the soil immediately adjacent to the skirts; indicating a general shear  
362 type reverse end bearing mechanism as opposed to a local pullout failure.

363 On tracing the vectors, it can be seen that while a similar volume of soil is mobilized  
364 beneath tip level at failure, different mechanisms accompany failure in compression  
365 and uplift. A Prandtl-type mechanism is evident in the displacement vectors shown in  
366 Fig. 5 for the foundations in compression whereas more of a Hill-type mechanism is  
367 evident for the foundations in uplift, particularly at low embedment. A schematic  
368 representation of Prandtl and Hill-type failures is shown in Fig. 6. A detailed

369 discussion of the failure mechanisms observed through PIV analysis of the centrifuge  
370 tests is presented by Mana et al. (2012a). The LDFE analyses capture the differences  
371 in the kinematic mechanisms in uplift and compression in line with the observed  
372 mechanisms.

373 The failure mechanisms can be scrutinized in more detail when presented as contours  
374 of displacement as shown in Fig. 7. The figure compares displacement contours in  
375 compression and uplift predicted by the LDFE analyses (right half) and observed from  
376 PIV analysis of the centrifuge tests (left half) for each of the skirt embedment ratios.  
377 Contours are plotted at intervals of 10 % of an incremental foundation displacement  
378 post-peak in uplift and at steady state in compression. For a given embedment ratio  
379 and load path, the contours from the LDFE analyses represent the same total  
380 foundation displacement as the contours from the equivalent PIV analysis of the  
381 centrifuge tests.

382 The contour plots show that the LDFE analyses predicted failure mechanisms that are  
383 broadly consistent with those observed in the centrifuge tests. An exception is the case  
384 of the deepest embedment ratio,  $d/D = 0.5$  in compression, for which the LDFE  
385 analysis predicted a similar mechanism in compression and uplift and failed to capture  
386 the confined mechanism (i.e. not extending to the soil surface) observed in  
387 compression in the centrifuge tests. Overall, the LDFE analyses captured the  
388 differences in failure mechanism in uplift and compression for a given foundation  
389 embedment ratio.

390 Fig. 8 compares displacement contours between SSFE and LDFE analyses for the  
391 foundation with embedment ratio  $d/D = 0.1$ . The SSFE analyses were carried out with  
392 equivalent geometry and soil parameters to the LDFE analyses. The SSFE analyses  
393 predict identical mechanisms in compression and uplift. Differences in the response



394 between uplift and compression cannot be captured by small strain finite element  
395 analysis since the geometry of the mesh is not updated and therefore the response in  
396 (fully bonded) uplift is by definition identical in nature to that in compression. Also,  
397 the Prandtl-type mechanism observed in compression in the centrifuge tests and the  
398 LDFE analysis is not evident in the SSFE result.

## 399 CONCLUDING REMARKS

400 This paper has demonstrated the potential of large deformation finite element (LDFE)  
401 analysis as a tool to predict the bearing response of shallow skirted foundations under  
402 undrained compression and uplift. LDFE analysis was used to back analyze centrifuge  
403 tests on shallow skirted foundations with a range of embedment ratios. The predicted  
404 response showed good agreement in terms of both predicted bearing capacity factor  
405 and failure mechanism.

406 The LDFE analyses predicted the full load-displacement response, pre- and post-  
407 yield. Changes in bearing capacity with foundation displacement were predicted,  
408 resulting from changing embedment ratio and local shear strength. Small strain  
409 analyses cannot capture this phenomenon in a single analysis. The LDFE analyses  
410 under-predicted the rate of change of bearing capacity with foundation displacement  
411 in uplift for low foundation embedment ratios. This is considered to be a result of the  
412 fully bonded skirt-soil interface underestimating the downward movement of the soil  
413 adjacent to the foundation skirt as the foundation displaces upwards. This downward  
414 movement increases the loss of embedment beyond that simply from foundation  
415 displacement, increasing the rate of reduction of bearing capacity with foundation  
416 displacement.

417 LDFE analyses were able to capture differences in failure mechanisms in undrained  
418 uplift and compression as observed from PIV analysis of centrifuge tests – a feature  
419 that cannot be captured by small strain finite element analyses.

420 The analyses reported in this paper have shown that LDFE techniques, coupled with  
421 an appropriate soil model, can capture the complete load-displacement behaviour and  
422 kinematic failure mechanisms observed during large movements of skirted  
423 foundations in undrained compression and uplift. The results presented increase  
424 confidence in using LDFE analysis to augment experimental test programmes to  
425 enable load paths or other site specific conditions to be considered that would be  
426 impossible or impractical to model experimentally.

427

## 428 ACKNOWLEDGEMENTS

429 The work described here forms part of the activities of the Centre for Offshore  
430 Foundation Systems, currently supported as a node of the Australian Research  
431 Council Centre of Excellence for Geotechnical Science and Engineering and the  
432 Lloyds Register Foundation. The work presented in this paper was supported through  
433 ARC grant DP0988904. This support is gratefully acknowledged.

## 434 REFERENCES

435

436 Andersen, K.H., Murff, J.D., Randolph, M.F., Clukey, E.C., Erbrich, C.T., Jostad,  
437 H.P., Hansen, B., Aubeny, C., Sharma, P. and Supachawarote, C. (2005). “Suction  
438 anchors for deepwater applications.” *Proc. 1st Int. Symp. Frontiers in Offshore*  
439 *Geotechnics (ISFOG)*, Perth, Australia, 1-30.

440 Biscontin, G., and Pestana, J. M. (2001). "Influence of peripheral velocity on vane  
441 shear strength of an artificial clay." *Geotech. Test. J.*, 24(4), 423-429.

442 Bye, A., Erbrich, C., Rognlien, B., and Tjelta, T.I. (1995). "Geotechnical design of  
443 bucket foundations." *Proc. Annual Offshore Technology Conf.*, Houston, OTC  
444 7793.

445 Chatterjee, S., Randolph, M. F., and White, D. J. (2012). "The effects of penetration  
446 rate and strain softening on the vertical penetration resistance of seabed pipelines."  
447 *Géotechnique*, 62(7), 573-582.

448 Christophersen, H.P., Bysveen, S., and Støve, O.J. (1992). "Innovative Foundation  
449 Systems Selected for the Snorre Field Development." *Proc. 6<sup>th</sup> International  
450 Conference on the Behavior of Offshore Structures (BOSS)*, 1, 81-94.

451 Dassault Systèmes (2010). "*Abaqus analysis users' manual.*" Simula Corp,  
452 Providence, RI, USA.

453 Dendani, H., and Colliat, J-L. (2002). "Girassol: design analyses and installation of  
454 the suction anchors." *Proc. Annual Offshore Tech. Conf.*, Houston, OTC 14209.

455 Einav, I., and Randolph, M. F. (2005). "Combining upper bound and strain path  
456 methods for evaluating penetration resistance." *Int. J. Numer. Methods Eng.*,  
457 63(14), 1991- 2016.

458 Erbrich, C. T. (2005). "Australian frontiers – spudcans on the edge." *Proc. 1st Int.  
459 Symp. on Frontiers in Offshore Geotechnics*, Perth, 49-74.

460 Gaudin, C., Mohr, H., Cassidy, M. J., Bienen, B., and Purwana, O. A. (2011).  
461 "Centrifuge experiments of a hybrid foundation under combined loading." *Proc.  
462 21<sup>st</sup> Int. Off. Pol. Engng. Conf. (ISOPE)*, Hawaii, USA.

463 Ghosh, S. and Kikuchi, N. (1991). "An arbitrary Lagrangian-Eulerian finite element  
464 method for large deformation analysis of elastic-viscoplastic solids." *Comput.*  
465 *Methods Appl. Mech. Eng.* 86(2), 127-188.

466 Gourvenec, S. M., Acosta-Martinez, H. E., and Randolph, M. F. (2009).  
467 "Experimental study of uplift resistance of shallow skirted foundations in clay  
468 under transient and sustained concentric loading." *Géotechnique*, 59(6), 525-537.

469 Gourvenec, S., and Barnett, S. (2011). "Undrained failure envelope for skirted  
470 foundations under general loading." *Géotechnique*, 61(3), 263-270.

471 Gourvenec, S., and Mana, D. S. K. (2011). "Undrained vertical bearing capacity  
472 factors for shallow foundations." *Géotechnique Letters*, 1(4), 101-108.

473 Hossain, M. S. and Randolph, M. F. (2010). "Deep-penetrating spudcan foundations  
474 on layered clays: numerical analysis." *Géotechnique* 60(3), 171-184.

475 Hu, Y., and Randolph, M. F. (1998a). "A practical numerical approach for large  
476 deformation problems in soil." *Int. J. Numer. Analyt. Meth. Geomech.*, 22(5), 327-  
477 350.

478 Hu, Y., and Randolph, M. F. (1998b). "*H*-adaptive FE analysis of elastoplastic  
479 nonhomogeneous soil with large deformation." *Comput. Geotech.* 23(1-2), 61-83.

480 Hu, Y., Randolph, M. F. and Watson, P. G. (1999). "Bearing response of skirted  
481 foundation on nonhomogeneous soil." *J. Geotech. Geoenviron. Engng, ASCE*,  
482 125(11), 924-935.

483 Lunne, T., Berre, T., Andersen, K. H., Strandvik, S., and Sjurset, M. (2006). "Effects  
484 of sample disturbance and consolidation procedures on measured shear strength of  
485 soft marine Norwegian clays." *Can. Geotech. J.*, 43(7), 726- 750.

486 Lunne, T., and Andersen, K. H. (2007). "Soft clay shear strength parameters for  
487 deepwater geotechnical design." *Proc. 6th Int. Offshore Site Investigation and*

488 *Geotechnics Conf.: Confronting New Challenges and Sharing Knowledge*, Society  
489 for Underwater Technology, London, 1, 151-176.

490 Mana, D. S. K., Gourvenec, S. M., Hossain, M. S., and Randolph, M. F. (2011).  
491 “Experimental investigation of the undrained response of a shallow skirted  
492 foundation subjected to vertical compression and uplift.” *Proc. 30<sup>th</sup> Int. Conf.*  
493 *Ocean Off. Arctic Engng (OMAE)*, Rotterdam, The Netherlands, OMAE2011-  
494 49072, 771-778.

495 Mana, D. S. K., Gourvenec, S. M., Randolph, M. F., and Hossain, M. S. (2012a).  
496 “Failure mechanisms of skirted foundations in uplift and compression.” *Int. J.*  
497 *Phy. Mod. Geotech. (IJPMG)*, 12(2), 47-62.

498 Mana, D. S. K., Gourvenec, S. M. and Randolph, M. F. (2012b). “An experimental  
499 investigation of reverse end bearing of offshore shallow foundations.” *Submitted*  
500 *to Canadian Geotechnical Journal*.

501 Martin, C. M. (2001). “Vertical bearing capacity of skirted circular foundations on  
502 Tresca soil.” *Proc. 15<sup>th</sup> Int. Conf. on Soil Mechanics and Geotechnical*  
503 *Engineering*, Istanbul, 1, 743-746.

504 Miller, D. M., Frazer, I., and Brevig, P. (1996). “The Heidrun Field – Marine  
505 Operations.” *Proc. Annual Offshore Technology Conf.*, Houston, OTC 8101.

506 Puech, A., Iorio, J.-P., Garnier, J., and Foray, P. (1993). “Experimental study of  
507 suction effects under mudmat type foundations.” *Proc. Canadian Conference on*  
508 *Marine Geotechnical Engineering*. St. John's, Newfoundland, 3, 1062-1080.

509 Randolph, M. F. (2004). “Characterization of soft sediments for offshore applications.  
510 Keynote Lecture.” *Proc. 2nd Int. Conf. on Site Characterization*, Porto, Portugal,  
511 1, Millpress Science Publishers, Rotterdam, 209-231.

512 Supachawarote, C., Randolph, M. F., and Gourvenec, S. (2004). "Inclined pullout  
513 capacity of suction caissons." *Proc. 14<sup>th</sup> Int. Offshore and Polar Eng. Conf.*,  
514 Toulon, France, 500-506.

515 Wang, D., White, D. J., and Randolph, M. F. (2010a). "Large deformation finite  
516 element analysis of pipe penetration and large-amplitude lateral displacement."  
517 *Can. Geotech. J.*, 47(8), 842-856.

518 Wang, D., Hu, Y. and Randolph, M. F. (2010b). "Three-dimensional large  
519 deformation finite-element analysis of plate anchors in uniform clay." *J. Geotech.*  
520 *Geoenviron. Engng, ASCE*, 136(2), 355-365.

521 Watson, P. G., Randolph, M. F., and Bransby, M. F (2000). "Combined lateral and  
522 vertical loading of caisson foundations." *Proc. Annual Offshore Technology Conf.*,  
523 Houston, OTC 12195.

524 Watson, P. G., and Humpheson, C. (2007). "Foundation design and installation of the  
525 Yolla-A platform." *Proc. 6<sup>th</sup> Int. Offshore Site Investigation and Geotechnics*  
526 *Conf. Soc. for Underwater Technology*, London, UK, 399-412.

527 White, D. J., Take, W. A. and Bolton, M. D. (2003). "Soil deformation measurement  
528 using Particle Image Velocimetry (PIV) and photogrammetry." *Géotechnique*,  
529 53(7), 619-631.

530 Zhou, H. and Randolph, M. F. (2006). "Large deformation analysis of suction caisson  
531 installation in clay." *Can. Geotech. J.* 43(12), 1344-1357.

532 Zhou, H., and Randolph, M. F. (2007). "Computational techniques and shear band  
533 development for cylindrical and spherical penetrometers in strain-softening clay."  
534 *Int. J. Geomech.*, 7(4), 287-295.

535

536

537 **Table 1. Parameters used in LDFE analysis**

| Parameters   | Values   |
|--|--|
| <i>Foundation:</i>   |  |
| Foundation diameter, D   | 12 m   |
| Skirt embedment depths, d  | 1.2 m, 2.4 m, 3.6 m & 6 m<br>(d/D = 0.1, 0.2, 0.3 & 0.5) |
| Skirt wall thickness, t  | 0.1 m (t/D = 0.008)                                      |
| Skirt-soil interface   | Fully rough  |
| <i>Soil:</i>   |  |
| Shear strength of soil at mudline, $s_{um}$  | 7.0 kPa  |
| Shear strength gradient, k   | 1.3 kPa/m  |
| Submerged unit weight of soil, $\gamma'$   | 7.0 kN/m <sup>3</sup>                                    |
| Stiffness ratio, $E_u/s_u$   | 400 (100 & 1000)   |
| Poisson's ratio, $\nu_u$   | 0.49   |
| <i>Strain rate and softening:</i>  |  |
| Reference shear strain rate, $\dot{\gamma}_{ref}$  | $3 \times 10^{-6} \text{ s}^{-1}$                        |
| Vertical skirt penetration rate, $v_f$   | 0.0001 m/s   |
| Incremental foundation displacement, $\delta$  | 0.08 % D   |
| Rate of strength increase per decade, $\mu$  | 0.1  |
| Sensitivity of clay, $S_t$   | 2.7  |
| Accumulated plastic strain at which 95 % soil strength reduction occurs by remolding, $\xi_{95}$ | 10   |

538

539

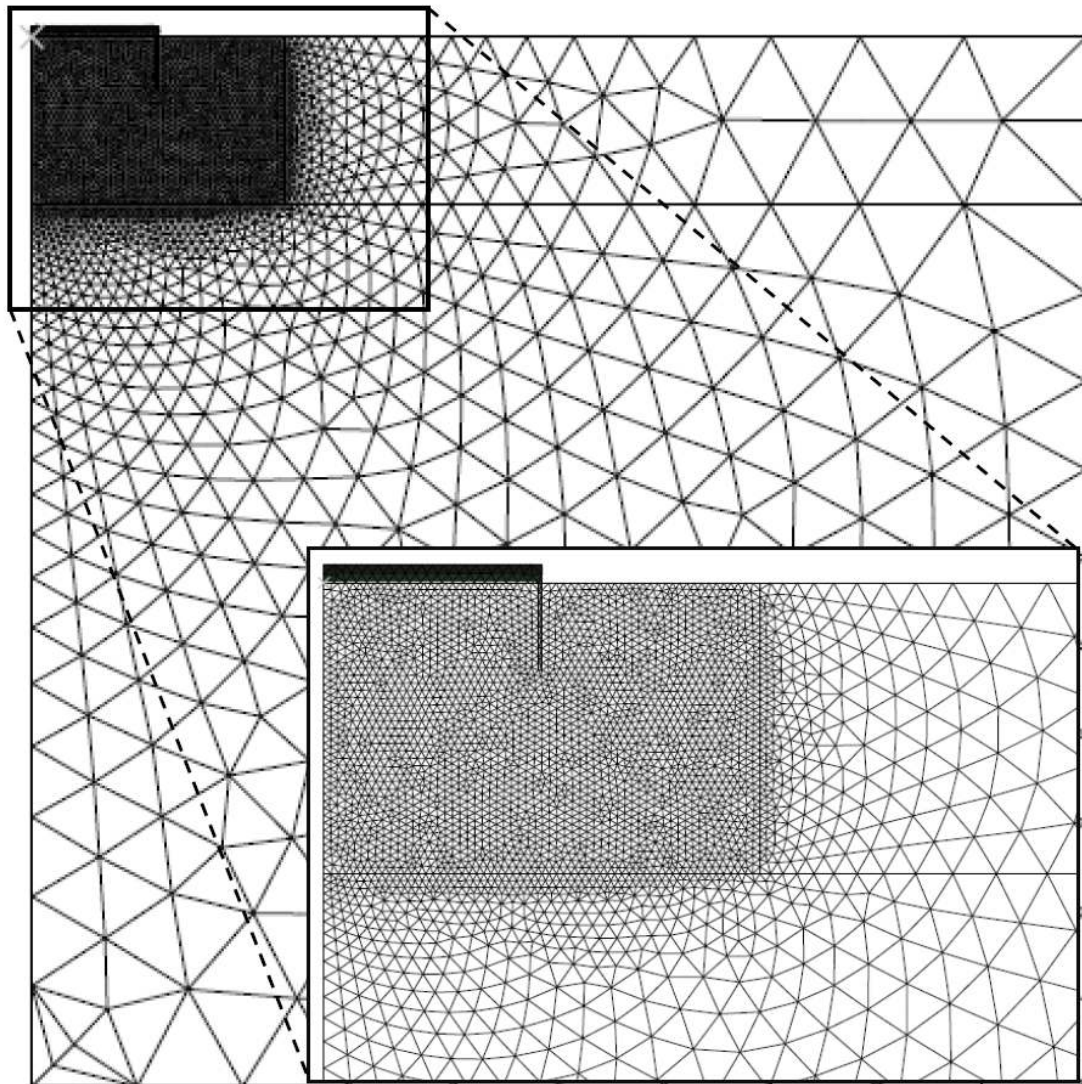
540 **Table 2. Summary of bearing capacity factors from centrifuge tests and LDFE**  
 541 **analysis compared with SSFE analysis and the theoretical solutions given by**  
 542 **Martin (2001)**  
 543

| <b>d/D</b> | <b>Bearing capacity factor, <math>N_{c0}</math></b> |             |           |           |                     |               |             |
|------------|---|-------------|-----------|-----------|---------------------|---------------|-------------|
|            | <b>Compression*</b>                                 |             |           |           | <b>Uplift (w/D)</b> |               | <b>SSFE</b> |
|            | <b>Centrifuge</b>                                   | <b>LDFE</b> | <b>LB</b> | <b>UB</b> | <b>Centrifuge</b>   | <b>LDFE</b>   |             |
| 0.1        | 9.17  | 9.24        | 8.05      | 9.50      | 8.00 (0.020)        | 8.88 (0.024)  | 8.8         |
| 0.2        | 10.18   | 9.63        | 8.50      | 10.50     | 9.30 (0.030)        | 9.33 (0.034)  | 9.55        |
| 0.3        | 10.67   | 9.92        | 8.90      | 11.05     | 9.80 (0.045)        | 9.62 (0.040)  | 10.1        |
| 0.5        | 11.38   | 10.18       | 9.45      | 12.50     | 10.85 (0.047)       | 10.03 (0.048) | 10.9        |

544 \*Compression capacity taken at a displacement w/D = 0.05 at which point a steady state had been  
 545 reached.  
 546  
 547



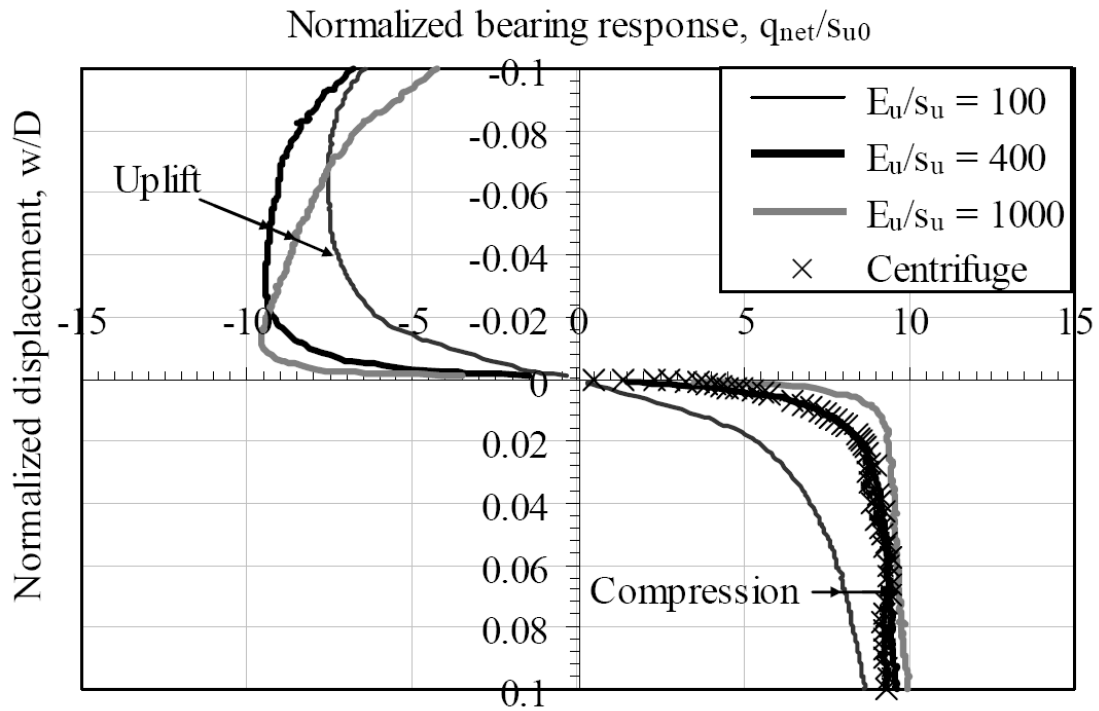
- 548 **List of figure captions**  
549  
550  
551 **Fig. 1. Finite element mesh used in LDFE analysis**  
552  
553 **Fig. 2. Variation of bearing capacity results with variation of (a) stiffness ratio**  
554  **$E_u/s_u$  (b) strain rate parameter  $\mu$  and (c) softening parameter  $\xi_{95}$  (all other**  
555 **parameters as in Table 1) for  $d/D = 0.1$**   
556  
557 **Fig. 3. (a ~ d) Comparison of bearing capacity factors for embedment ratios  $d/D$**   
558  **$= 0.1, 0.2, 0.3$  and  $0.5$  from LDFE and centrifuge tests**  
559  
560 **Fig. 4 Comparison of resistances between LDFE and centrifuge tests for  $d/D =$**   
561  **$0.5$ : (a)  $E/s_u = 500$ ; (b)  $\xi_{95} = 50$ ; (c)  $\mu = 0.2$**   
562  
563 **Fig. 5. Comparison of the displacement vectors for embedment ratios  $0.1$  &  $0.5$**   
564 **from LDFE and PIV analyses**  
565  
566 **Fig. 6 Difference in failure mechanism in compression and uplift**  
567  
568 **Fig. 7. Comparison of the normalized displacement contours from PIV and**  
569 **LDFE analyses**  
570  
571 **Fig. 8. Comparison of failure mechanisms predicted by SSFE and LDFE**  
572 **analyses ( $d/D = 0.1$ ): (a) Compression; (b) Uplift**



574  
575  
576  
577

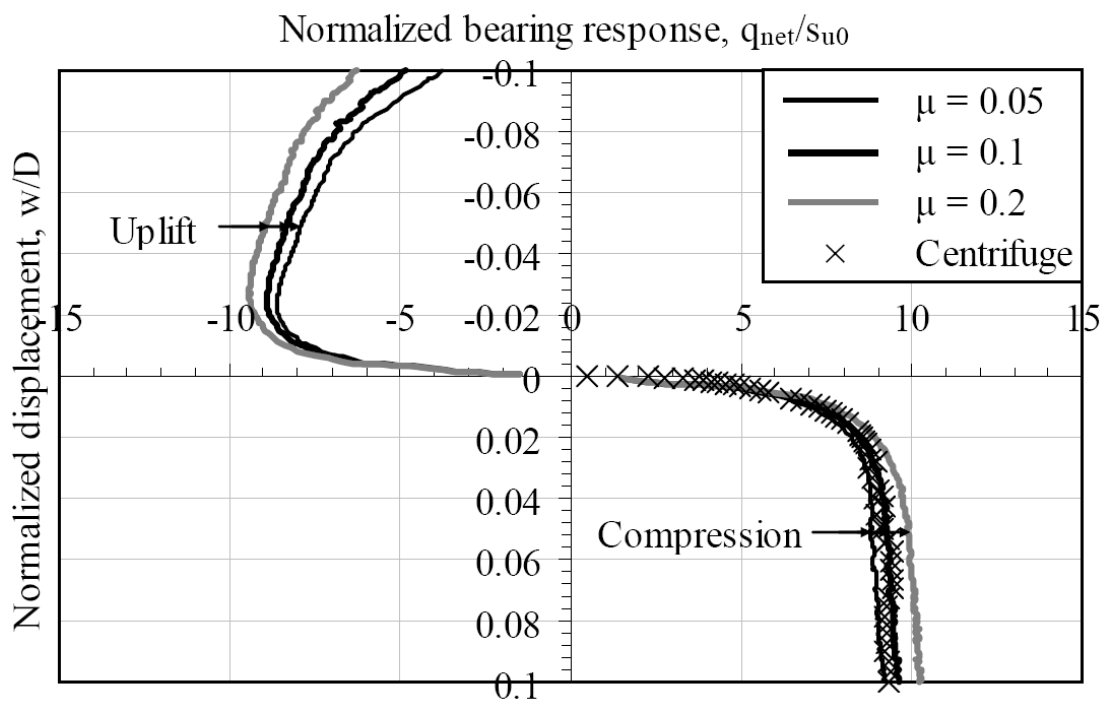
**Fig. 1. Finite element mesh used in LDFE analysis**

578



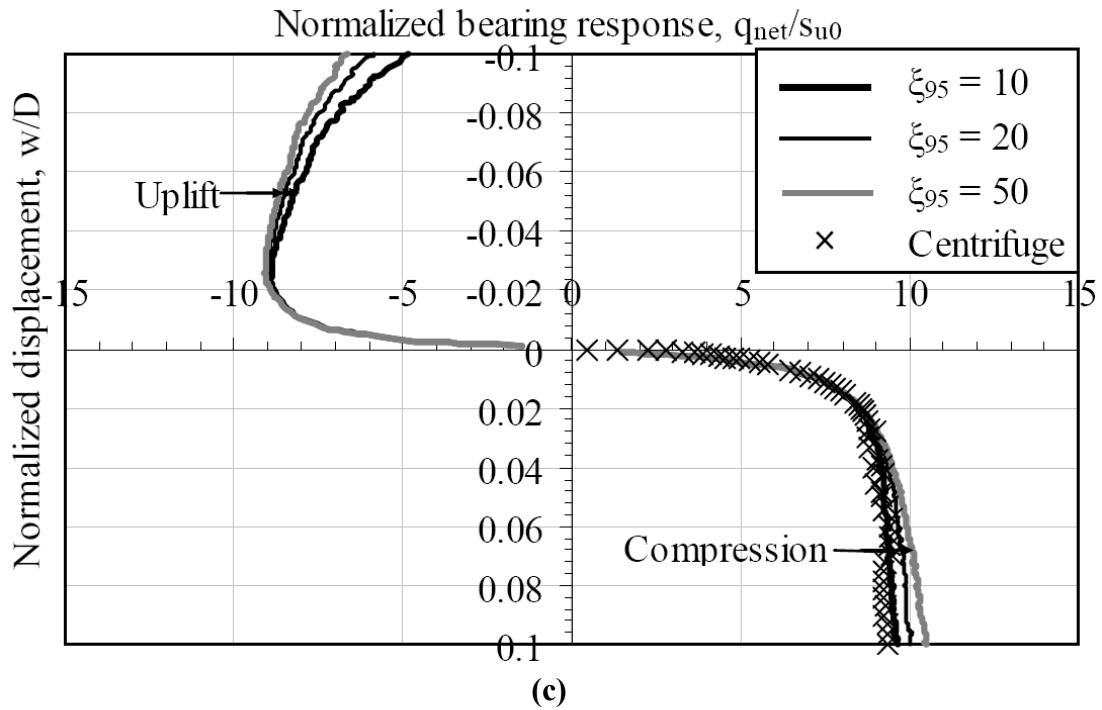
579  
580  
581

(a)



582  
583  
584  
585

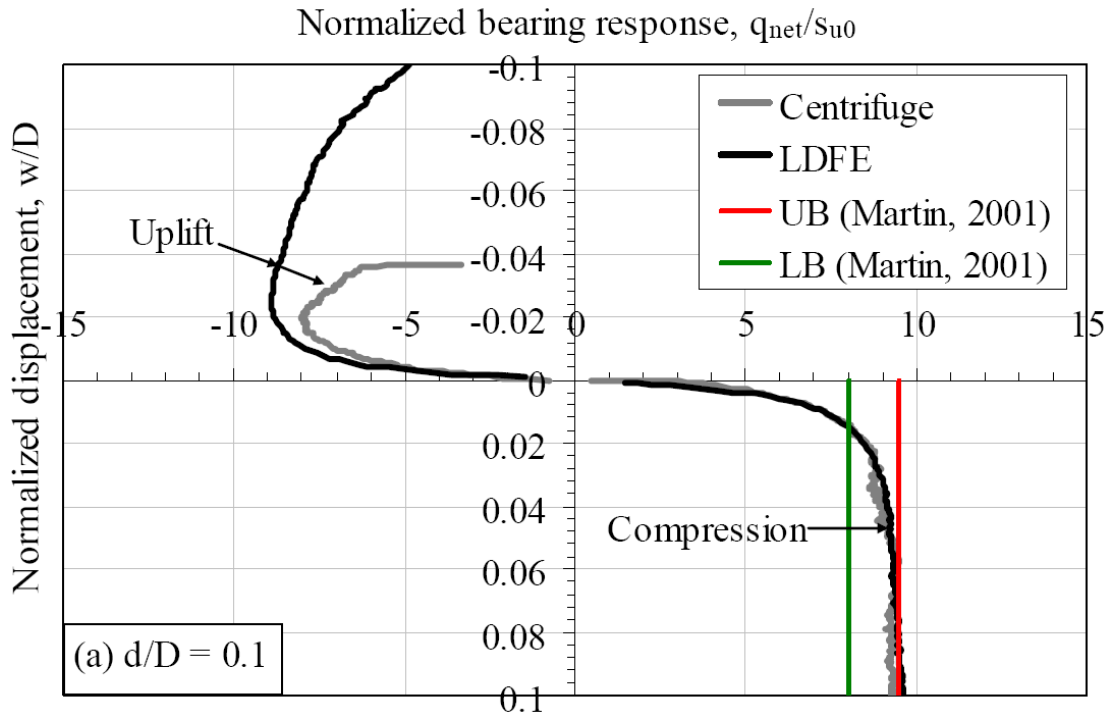
(b)



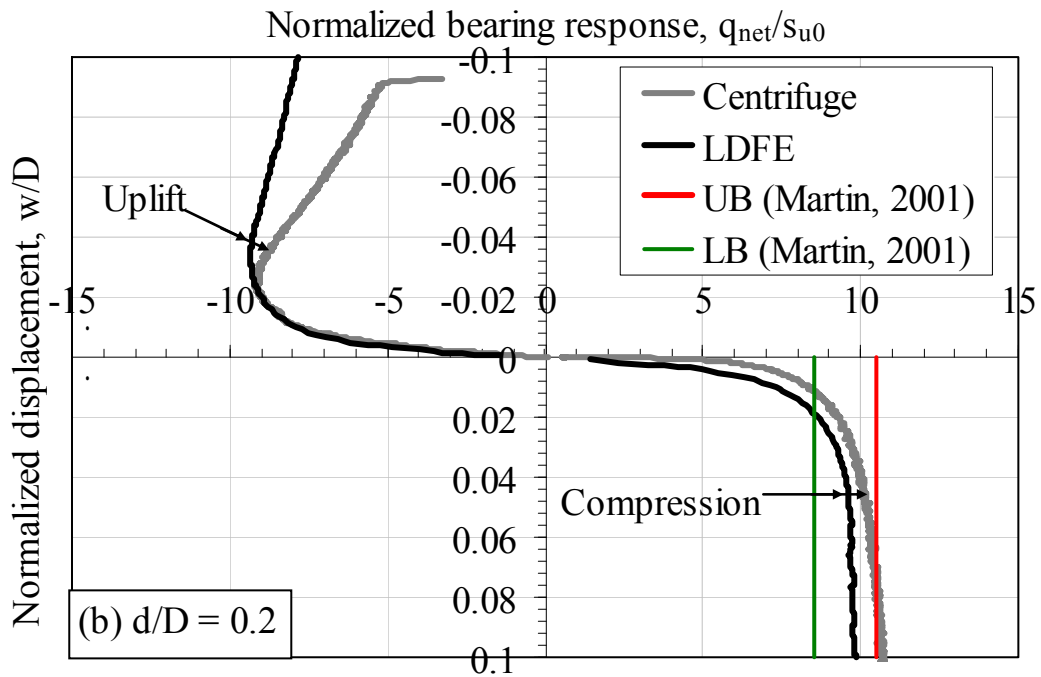
586  
 587  
 588  
 589  
 590  
 591  
 592

**Fig. 2. Variation of bearing capacity results with variation of (a) stiffness ratio  $E_u/s_u$  (b) strain rate parameter  $\mu$  and (c) softening parameter  $\xi_{95}$  (all other parameters as in Table 1) for  $d/D = 0.1$**

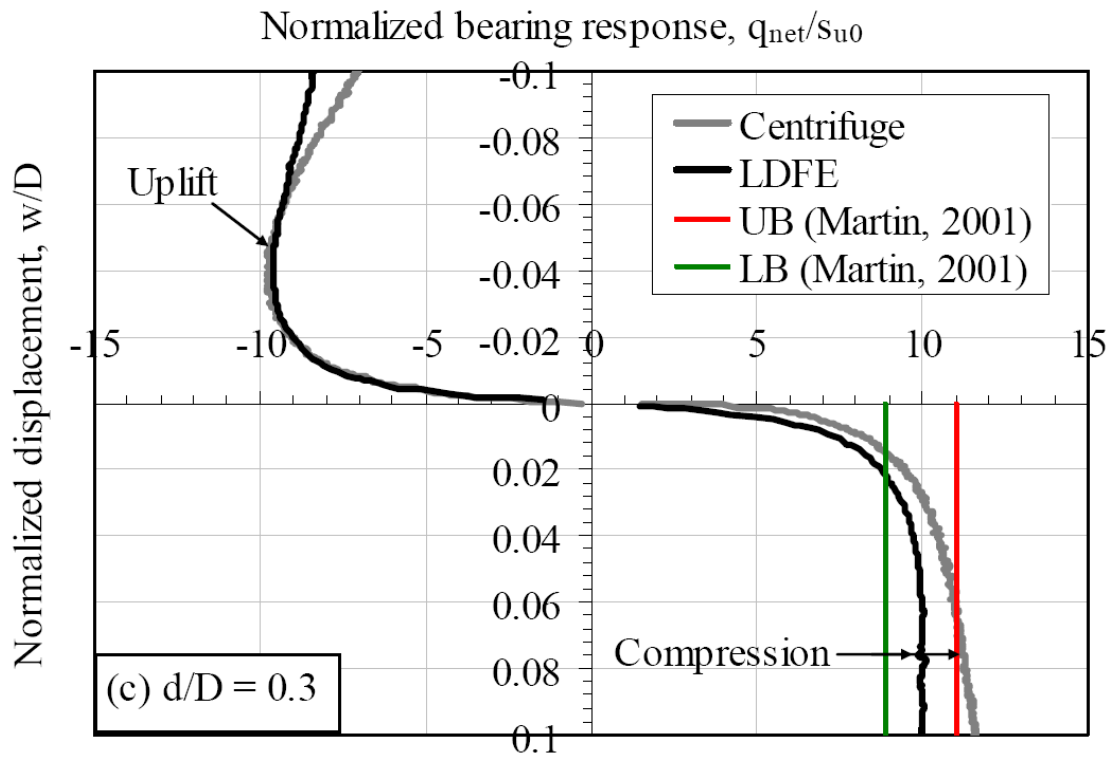
593



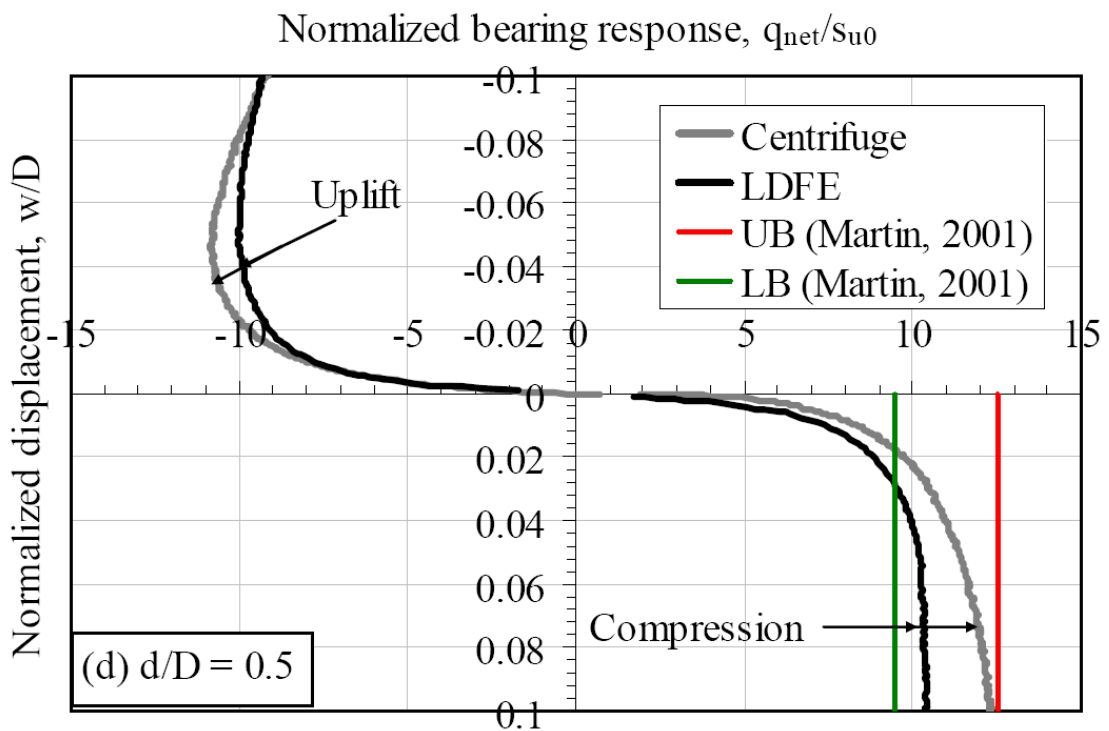
594  
595  
596



597

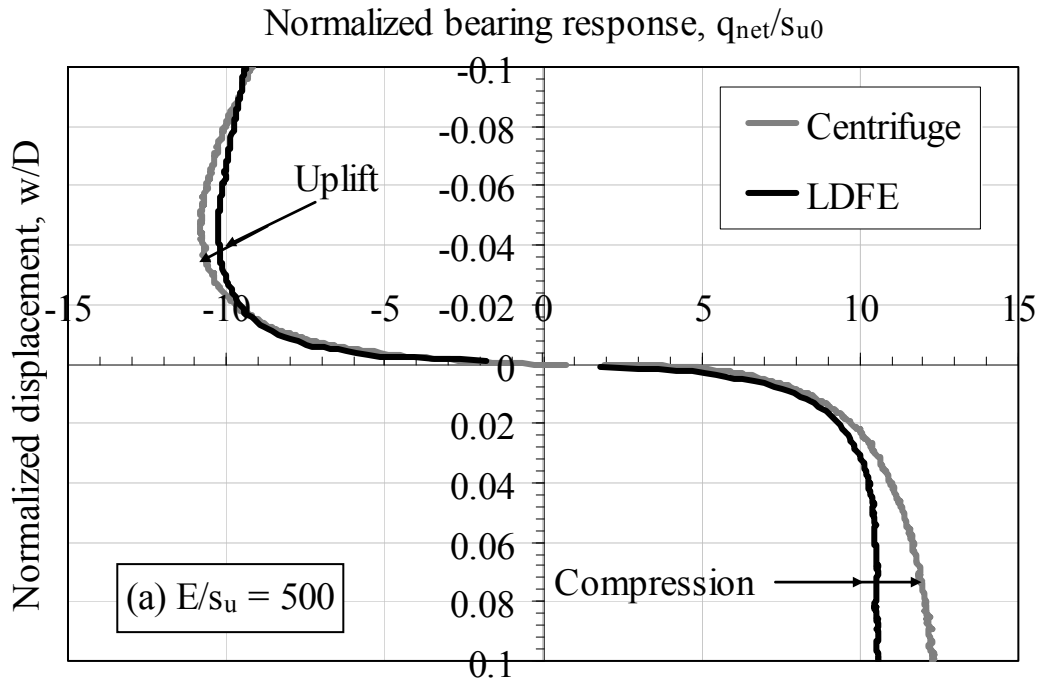


598

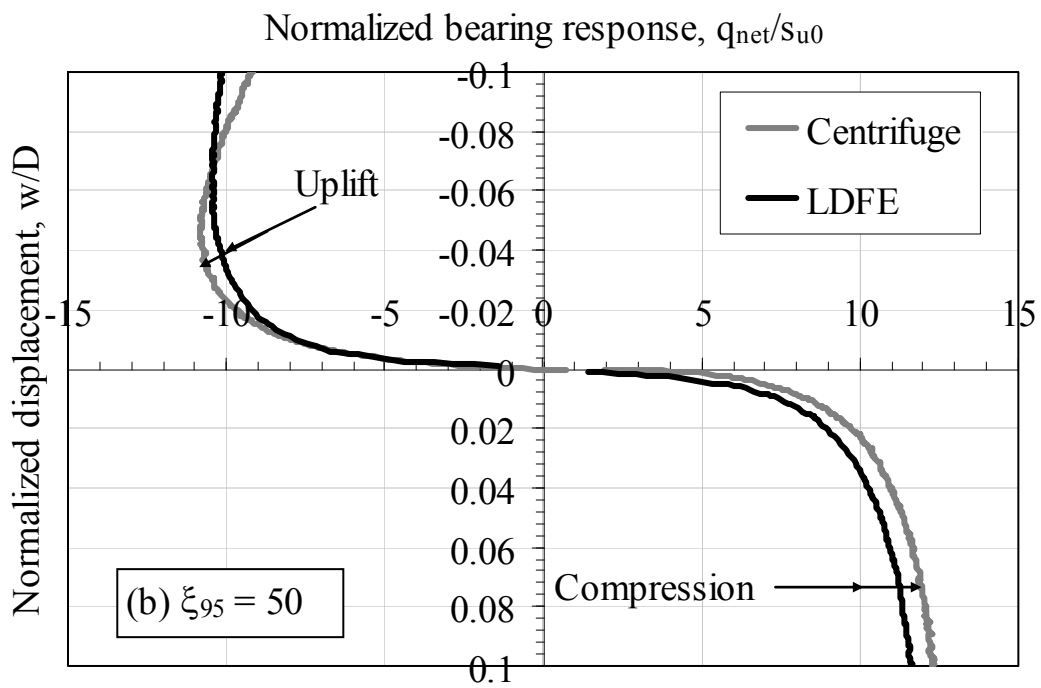


599

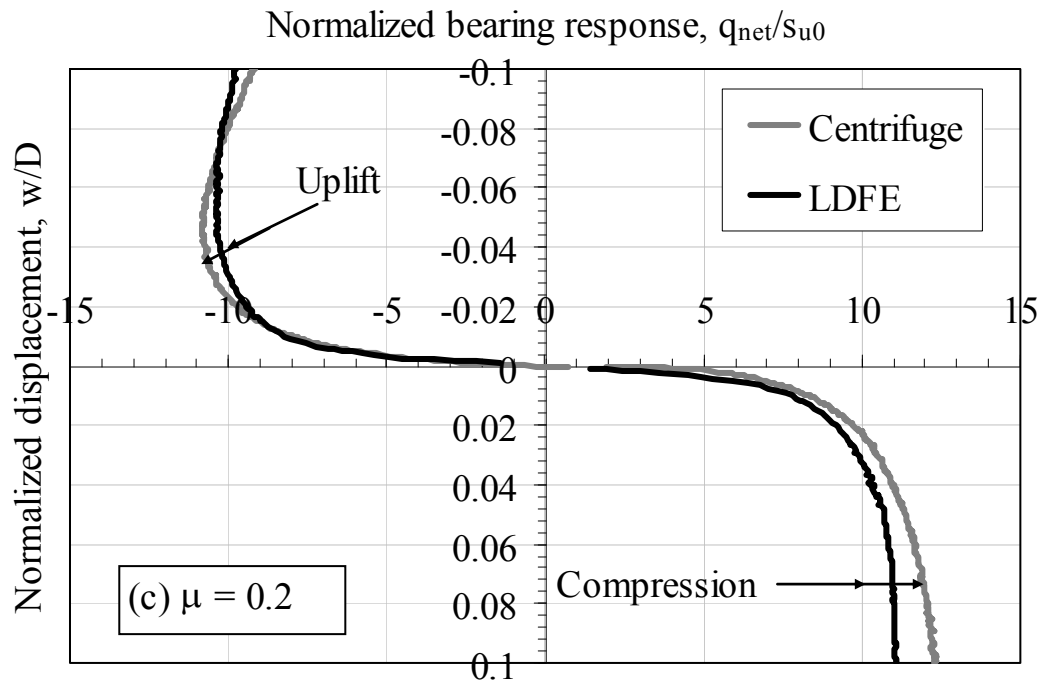
600 **Fig. 3. (a ~ d) Comparison of bearing capacity factors for embedment ratios  $d/D$**   
 601 **= 0.1, 0.2, 0.3 and 0.5 from LDFE and centrifuge tests**  
 602



603  
604



605  
606  
607

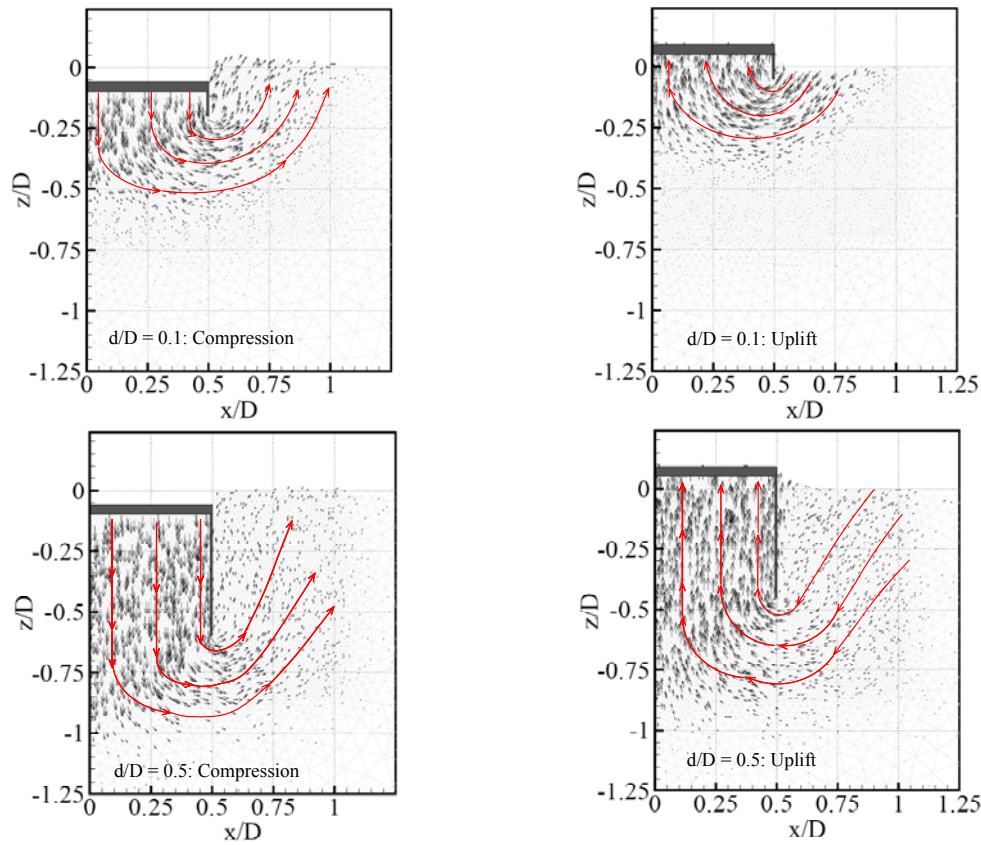


608  
 609  
 610  
 611

**Fig. 4 Comparison of resistances between LDFE and centrifuge tests for  $d/D = 0.5$ : (a)  $E/s_u = 500$ ; (b)  $\xi_{95} = 50$ ; (c)  $\mu = 0.2$**

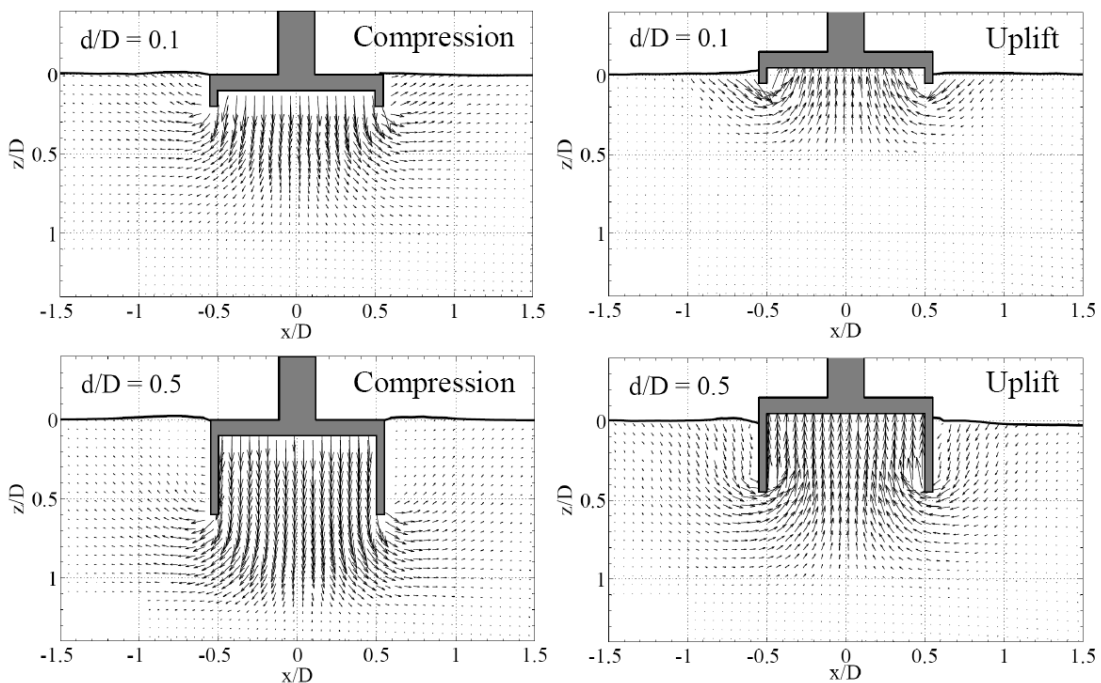


612



613  
614

**(a) LDFE analysis**

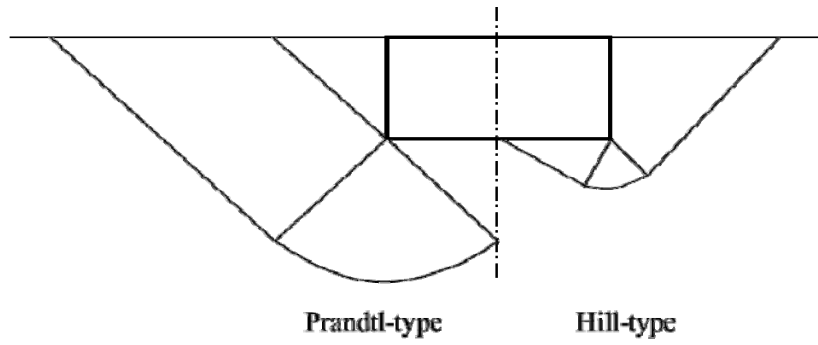


615  
616  
617  
618  
619  
620

**(b) PIV analysis**

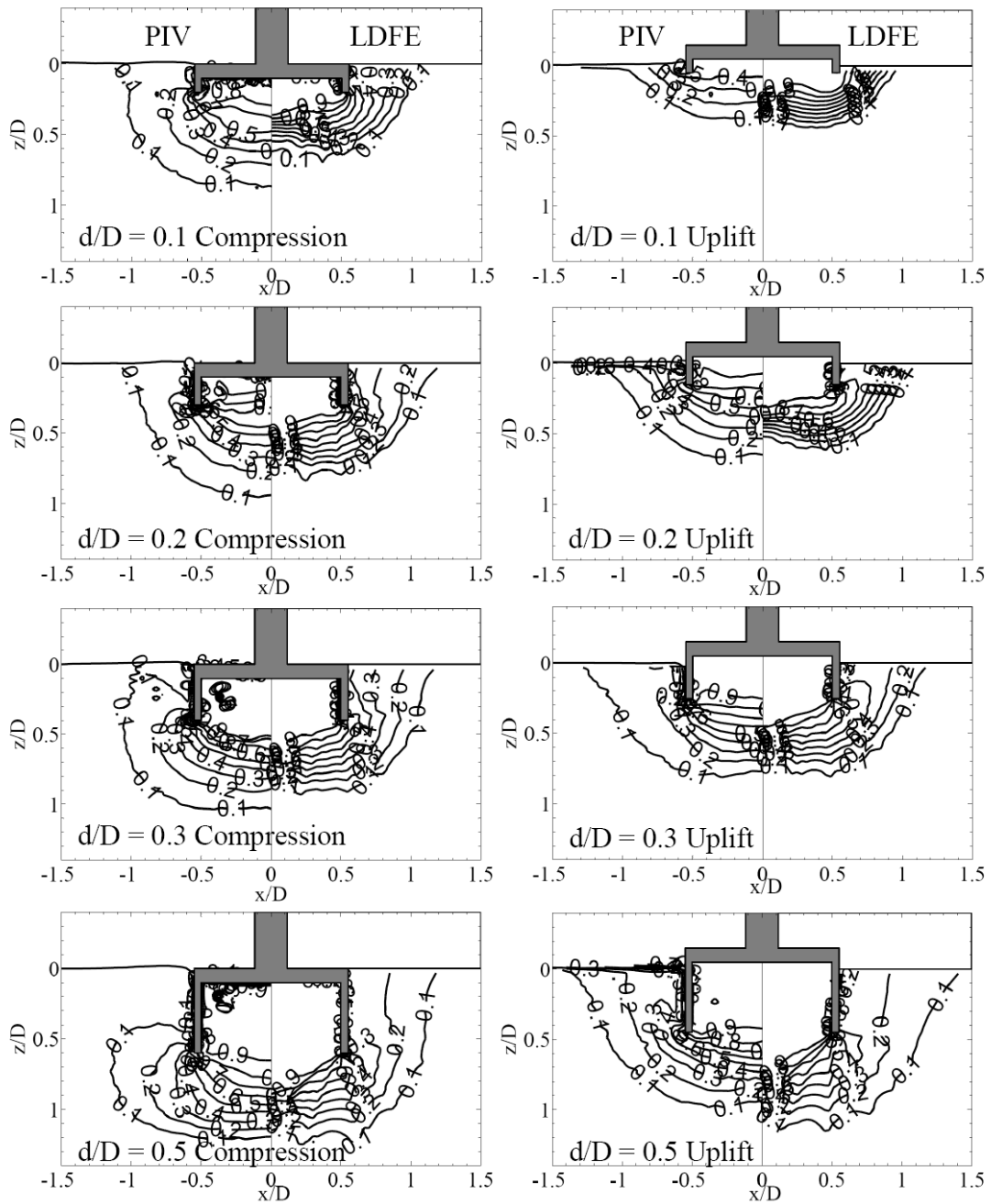
**Fig. 5. Comparison of the displacement vectors for embedment ratios 0.1 & 0.5 from LDFE and PIV analyses**

621  
622  
623  
624  
625



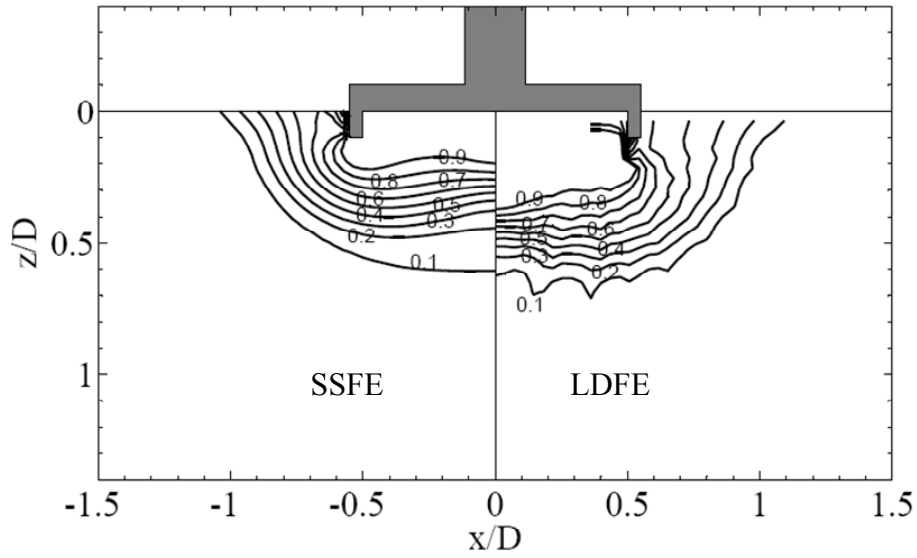
626  
627

**Fig. 6 Difference in failure mechanism in compression and uplift**



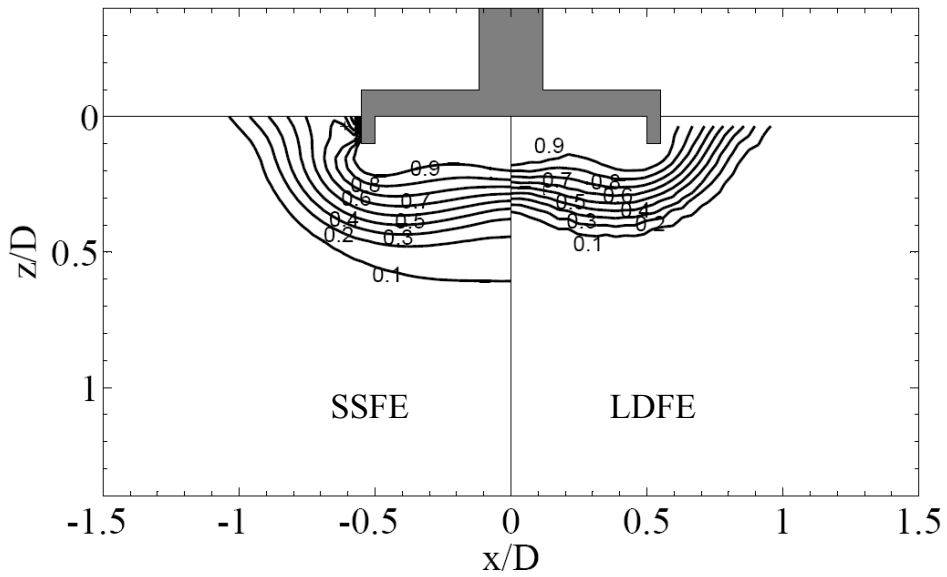
629  
 630  
 631  
 632  
 633  
 634  
 635  
 636  
 637  
 638  
 639  
 640  
 641  
 642

**Fig. 7. Comparison of the normalized displacement contours from PIV and LDFE analyses**



(a) Compression

643



(b) Uplift

644

645

646 **Fig. 8. Comparison of failure mechanisms predicted by SSFE and LDFE**  
 647 **analyses ( $d/D = 0.1$ ): (a) Compression; (b) Uplift**